Rayleigh–Taylor instability in cylindrical geometry with compressible fluids

Huidan Yu[1,a] and Daniel Livescu[2,b]
[1]*CCS-2/CNLS, Los Alamos National Laboratory, Los Alamos, New Mexico 87545, USA*
[2]*CCS-2, Los Alamos National Laboratory, Los Alamos, New Mexico 87545, USA*

(Received 25 March 2008; accepted 26 August 2008; published online 10 October 2008)

A linear stability analysis of the Rayleigh–Taylor instability (RTI) between two ideal inviscid immiscible compressible fluids in cylindrical geometry is performed. Three-dimensional (3D) cylindrical as well as two-dimensional (2D) axisymmetric and circular unperturbed interfaces are considered and compared to the Cartesian cases with planar interface. Focuses are on the effects of compressibility, geometry, and differences between the convergent (gravity acting inward) and divergent (gravity acting outward) cases on the early instability growth. Compressibility can be characterized by two independent parameters—a static Mach number based on the isothermal sound speed and the ratio of specific heats. For a steady initial unperturbed state, these have opposite influence, stabilization and destabilization, on the instability growth, similar to the Cartesian case [D. Livescu, Phys. Fluids **16**, 118 (2004)]. The instability is found to grow faster in the 3D cylindrical than in the Cartesian case in the convergent configuration but slower in the divergent configuration. In general, the direction of gravity has a profound influence in the cylindrical cases but marginal for planar interface. For the 3D cylindrical case, instability grows faster in the convergent than in the divergent arrangement. Similar results are obtained for the 2D axisymmetric case. However, as the flow transitions from the 3D cylindrical to the 2D circular case, the results above can be qualitatively different depending on the Atwood number, interface radius, and compressibility parameters. Thus, 2D circular calculations of RTI growth do not seem to be a good model for the fully 3D cylindrical case. © *2008 American Institute of Physics*.
[DOI: 10.1063/1.2991431]

I. INTRODUCTION

The Rayleigh–Taylor instability (RTI)[1,2] occurs at an interface between two fluids having different densities when the fluids are subjected to accelerations or body forces. In many cases, such as astrophysical situations, oceans, and atmosphere, the acceleration is due to gravity. If the acceleration points from the heavy to the light fluid, the interface between the two fluids is unstable. In this case any perturbation with a wavelength larger than the cutoff due to surface tension (for the immiscible case) or mass diffusion (for the miscible case) will grow. As the perturbation grows, smaller and larger wavenumbers are generated by nonlinear interactions and eventually the flow becomes turbulent. There is a complex phenomenology associated with the evolution of RTI including formation, competition, and amalgamation of spikes and bubbles, entrainment, and, eventually, turbulence. In general, the fluids can be immiscible or miscible; in the latter case the material mixing also influences the flow development. If the amplitudes of the initial perturbations are sufficiently small, the early stages of the instability growth can be described by the linearized governing equations.

For a planar interface (PI) in the Cartesian geometry, the linear growth rate for incompressible immiscible fluids is well known and has become a classic textbook result.[3] In this configuration, the role of compressibility on the linearized RTI development has been studied by a number of researchers. While Sharp[2] found a stabilizing effect of compressibility, other researchers[4–7] reported that compressibility has a destabilizing effect on RTI. This controversy was settled by Livescu,[8] who showed that compressibility can be characterized by two independent parameters, the isothermal speed of sound, c_T (which can be changed, for example, by varying the undisturbed pressure at the interface, p_0), and the ratio of specific heats, γ. For isothermal initial conditions, the perturbation growth rate decreases when p_0 decreases (more compressible flow) but increases when γ decreases (more compressible fluid), which clarifies the dual character, stabilizing and destabilizing, of compressibility reported in the literature. Incompressible limits are independently obtained when either $M \to 0$ or $\gamma \to \infty$, where M is the static Mach number (defined using the gravity wave speed and the isothermal speed of sound). The compressible to incompressible limit has been studied for the fully nonlinear equations when the pressure is a function of density only (barotropic case) in Ref. 9. In the case of $M \to 0$, global weak solutions of the incompressible Navier–Stokes equations[10] are recovered. On the other hand, as $\gamma \to \infty$, the incompressible limit may, in general, be different, underlying the nonuniqueness of the compressible to incompressible limit. No such result exists for the fully (nonisentropic) compressible nonlinear case, although the results highlighted above show that the linearized compressible equations in the Cartesian geometry do not have a single incompressible limit.

In many applications, RTI occurs in non-Cartesian geometries. For example, RTI plays an important role in super-

[a]Electronic mail: hyu@lanl.gov.
[b]Electronic mail: livescu@lanl.gov.

nova explosions, stellar pulsations,[11] or inertial confinement fusion (ICF).[12,13] Such systems with spherical or cylindrical geometries can be geometrically divergent (explosive) or convergent (implosive). In most situations the resulting flows are compressible. The effects of compressibility and geometry on the instability growth are, thus, of great interest.

When the instability occurs at a circular interface (CI) in cylindrical or spherical geometries, there are effects not present in the Cartesian case. In general, the perturbation growth can be due to the interface motion, a body force acting on the fluids, or a combination of both. In the usual ICF applications, both the ablative front and buoyancy force contribute to the instability at the interface. However, in many other applications, the instability can be dominated by the buoyancy effects (e.g., Ref. 14). Bell[15] was the first to study the perturbation growth due to an arbitrary radial motion of the interface in a cylindrical domain. The motion can be produced, for example, by an initial impulse or continuously driven by an external mechanism. In curved geometries, even the uniform motion of the interface leads to instability. Under an assumption that the flow is irrotational and of amplitude small compared to the wavelength of the perturbation, Bell derived differential equations for the amplitude of the perturbation as functions of time. Later, Plesset[16] derived the amplitude growth equation in a sphere based on the same incompressible flow methodology. These results are now referred to as the Bell–Plesset (BP) effect.[17,18] Recently, the BP treatment was employed in assessing the instability growth in different flow arrangements in both cylindrical and spherical geometries.[19–23] Studies based on the Euler equations assuming self-similar motion of the interface also exist for cylindrical[24,25] and spherical[26,27] geometries. Epstein[28] examined BP effects for an incompressible perturbation for planar, cylindrical, and spherical interfaces and demonstrated a clear distinction between the BP effect and RTI. Nevertheless, there are very few studies to address the contribution to the instability growth due to a RT mechanism in convergent geometries. An early work[29] introduced buoyancy to analyze RTI in an ablating plasma. A specific mathematical method for obtaining the dispersion relation and unstable mode profiles in spherical geometry was presented; however, the physical effects on RTI growth were not explored.

This paper aims to fill a gap in the present knowledge on the early development of RTI in cylindrical geometry. Focuses are on the effects of compressibility and geometry (including convergence/divergence effects) on the instability growth. The remainder of this paper is organized as follows. Section II introduces the linearized governing equations, including the zeroth- and first-order equations, and the incompressible limits. Analytical solutions are given in Sec. III. Section IV presents numerical results pertaining to three aspects: (1) compressibility effects, (2) geometry effects, and (3) differences between the convergent and divergent configurations. Section V provides a summary and conclusions.

II. LINEARIZED GOVERNING EQUATIONS

The problem considered here is stated as follows: two ideal inviscid immiscible compressible fluids in a cylindrical domain with coordinates r, θ, z are subject to a steady acceleration $\vec{g}=g\vec{e}_r$ in the radial direction. The interface between the two fluids is located at $r=r_0$. The densities of the two fluids at the interface are ρ_l (for the light fluid) and ρ_h (for the heavy fluid). There are two unstable RT configurations, with different arrangements of the fluids and directions of acceleration. The convergent case corresponds to infinite outer-layer heavy fluid versus finite confined light fluid with inward acceleration ($g<0$) and the divergent case is vice versa. In both cases, the normalized density difference defines the Atwood number, $A=(\rho_h-\rho_l)/(\rho_h+\rho_l)$.

The governing equations corresponding to mass, momentum, and energy conservation laws for each fluid are

$$\rho_{,t}+(r\rho u_r)_{,r}/r+(\rho u_\theta)_{,\theta}/r+(\rho u_z)_{,z}=0, \tag{1a}$$

$$r(\rho u_r)_{,t}+(r\rho u_r^2)_{,r}+(\rho u_r u_\theta)_{,\theta}+r(\rho u_r u_z)_{,z}-\rho u_\theta^2=-rp_{,r}+\rho g r, \tag{1b}$$

$$r(\rho u_\theta),t+(r\rho u_r u_\theta)_{,r}+(\rho u_\theta^2)_{,\theta}+r(\rho u_z u_\theta)_{,z}+\rho u_\theta u_r=-rp_{,\theta}, \tag{1c}$$

$$r(\rho u_z)_{,t}+(r\rho u_r u_z)_{,r}+(\rho u_z u_\theta)_{,\theta}+r(\rho u_z^2)_{,z}=-rp_{,z}, \tag{1d}$$

$$rp_{,t}+(rpu_r)_{,r}+(pu_\theta)_{,\theta}+r(pu_z)_{,z}=-(\gamma-1)\{(rq_r)_{,r}+q_{\theta,\theta}+rq_{z,r}+p_j[(ru_r)_{,r}+u_{\theta,\theta}+ru_{z,z}]\}, \tag{1e}$$

with ρ, $\vec{u}(u_r,u_\theta,u_z)$, p, and $\vec{q}(q_r,q_\theta,q_z)$ the density, velocity vector, pressure, and heat flux vector. $(\cdots)_{,f}$ is used to denote $\partial(\ldots)/\partial f$. The heat flux is expressed as $\vec{q}=-\lambda\nabla T$ with λ the thermal conductivity. The energy equation was written as Eq. (1e) by assuming ideal gas equation of state $p=R\rho T$ and caloric equation of state $e=c_vT=[R/(\gamma-1)]T$, where R is the gas constant, e is the internal energy, c_v is the specific heat at constant volume, and γ is the ratio of specific heats.

A. Zeroth-order equations

Let $\rho^{(0)}$, $u_r^{(0)}$, $p^{(0)}$, and $T^{(0)}$ be the variables defining the equilibrium state. As mentioned in Sec. I, the instability of the interface can be produced by an acceleration $g(r)$ as well as interface movement $u^{(0)}$ or a combination of both. In this paper, we focus on the classical RTI by setting $u^{(0)}=0$. Thus, the fluids are initially at rest, separated by a perfectly cylindrical unperturbed interface, and subjected to a constant and uniform acceleration g.

With these assumptions, the zeroth-order equations for fluid j, where $j=l,h$, reduce to

$$\rho_{j,t}^{(0)}=0, \tag{2a}$$

$$p_{j,r}^{(0)}=g\rho_j^{(0)}, \quad p_{j,\theta}^{(0)}=p_{j,z}^{(0)}=0, \tag{2b}$$

$$p_{j,t}^{(0)}=(\gamma_j-1)(\lambda_j T_{j,r}^{(0)})_{,r}/\gamma_j. \tag{2c}$$

We further assume that the equilibrium state is steady and λ_j is constant. Then the energy equation becomes $T^{(0)}_{j,r}=0$. For infinite domain, as the temperature needs to be bounded, this yields that the outer fluid has constant temperature. Assuming that the derivatives are continuous inside each of the fluid domains, we obtain that the temperature of the inner fluid is also constant. Since the two fluids are in thermal equilibrium, this yields uniform temperature in the whole domain. Thus, the equilibrium state of fluid j is given by

$$T^{(0)}_j = T_0, \tag{3a}$$

$$p^{(0)}_j = p_0 e^{g(r-r_0)/R_jT_0}, \tag{3b}$$

$$\rho^{(0)}_j = \frac{p_0}{R_jT_0} e^{g(r-r_0)/R_jT_0}, \tag{3c}$$

where p_0 is the unperturbed pressure at the interface. The zeroth-order equation of state is $p^{(0)}_j=\rho^{(0)}_j R_jT_0$.

B. First-order equations

The interface between the two fluids is perturbed with a small amplitude perturbation so that the primary variables can be decomposed as the sum between the equilibrium values and some small perturbations, ρ', u'_r, u'_θ, u'_z, p', and T'. The decomposition is plugged into the governing equations and, after all quadratic or higher order terms in the perturbations are neglected, the first-order equations are obtained as

$$\rho'_{,t} + \rho^{(0)}(\nabla\cdot\vec{u}') + u'_r\rho^{(0)}_{,r} = 0, \tag{4a}$$

$$\rho^{(0)}u'_{r,t} = -p'_{,r} + g\rho', \tag{4b}$$

$$r\rho^{(0)}u'_{\theta,t} = -p'_{,\theta}, \tag{4c}$$

$$\rho^{(0)}u'_{z,t} = -p'_{,z}, \tag{4d}$$

$$p'_{,t} + u'_r p^{(0)}_{,r} = -\gamma p^{(0)}(\nabla\cdot\vec{u}'), \tag{4e}$$

with $\nabla\cdot\vec{u}=(ru'_r)_{,r}/r+u'_{\theta,\theta}/r+u'_{z,z}$. Thermal conduction is neglected in the first-order equations as the effects are small when the zeroth-order state is in thermal equilibrium. Equations (4a)–(4e) are written formally for the entire domain so that the variables are generalized functions as the density is discontinuous across the interface. However, the equations are solved separately for each fluid and integrated over the interface to get a jump conditions. This method avoids dealing directly with delta functions. Besides the jump condition, the other boundary conditions needed are at $r=0$ and $r\to\infty$ that are discussed below.

From the energy equation [Eq. (4e)], it can be seen that $\gamma p^{(0)}\to\infty$ leads to $\nabla\cdot\vec{u}=0$ which defines the incompressible limit. Thus, there exist two types of incompressible limits: as $p^{(0)}\to\infty$ with finite γ and as $\gamma\to\infty$ with finite $p^{(0)}$, similar to the fully compressible linear Cartesian case[8] and consistent with the barotropic nonlinear equations.[9] For both limits, $c_s\to\infty$ for finite $\rho^{(0)}$, where $c_s=\sqrt{\gamma p^{(0)}/\rho^{(0)}}$ is the sound speed. Nevertheless, the two limits may be different, so that $c_s\to\infty$ is not unique. Thus, in general, compressibility can be characterized by two independent parameters, one related to the flow (p_0) and the other a property of the fluid (γ). Since for the problem considered here the density is fixed, the limit $p^{(0)}\to\infty$ also leads to $T^{(0)}\to\infty$, resulting in spatial uniform density, as can be seen from Eq. (3b), whereas $\gamma\to\infty$ allows spatially varying density, $\rho^{(0)}=\rho^{(0)}(r)$. Similar limiting cases are obtained for a PI in the Cartesian system.[8] For the sake of brevity, in the rest of the paper we use the abbreviations UDIL for uniform density incompressible limit and VDIL for varying density incompressible limit.

It is known that for ideal gases γ does not exceed 5/3. However, there are two situations that allow, formally, to consider larger values for γ. First, in the absence of viscous effects and heat sources, the flow is isentropic. For ideal gas, the energy equation (1e) reduces to

$$\frac{d(p'+p^{(0)})}{p'+p^{(0)}} = \gamma\frac{d(\rho'+\rho^{(0)})}{\rho'+\rho^{(0)}}, \tag{5}$$

which is the so called γ-law. More generally, Eq. (5) can describe a polytropic transformation if γ is replaced by the polytropic exponent β. In this case, Eq. (5) can still replace the energy equation after a consistent source or sink of energy is added in [see Ref. 30]. Thus, the exponent can have any real value if a polytropic process is considered. Second, many liquids can be treated as γ-law gases with large value of γ in certain thermodynamic conditions, again with Eq. (5) replacing the energy equation.[31]

III. ANALYTICAL SOLUTIONS

Following the standard procedure,[3] we seek solutions for the perturbations ρ', p', u'_r, u'_θ, and u'_z whose dependence on θ, z, and t has the form $e^{i(m\theta+k_zz)+nt}$. Here n is the growth rate of the perturbation, m is an integer representing the number of waves in the θ direction, and k_z is the wavenumber in the z direction. The wavenumber in the θ direction is $k_\theta=m/r_0$ and depends on the position of the interface.

After substituting $f'(r,\theta,z,t)=f(r)e^{i(m\theta+k_zz)+nt}$ with f representing ρ, p, u_r, u_θ, and u_z into the first-order equations (4a)–(4e), one obtains

$$n\rho + b\rho^{(0)}u_r + \rho^{(0)}\Delta = 0,$$

$$\rho^{(0)}nu_r = -Dp + g\rho,$$

$$r\rho^{(0)}nu_\theta = -imp,$$

$$\rho^{(0)}nu_z\theta = -ik_zp,$$

$$np + a\rho^{(0)}u_r = -c_s^2\rho^{(0)}\Delta,$$

where $b=g/RT^{(0)}$ and the divergence of velocity fluctuations is given by $\Delta=Du_r+u_r/r+imu_\theta/r+ik_zu_\theta$ with $D\equiv d/dr$. After eliminating ρ, p, u_θ, and u_z, one obtains an equation for u_r:

$$\rho^{(0)}u_r-\frac{g\rho^{(0)}[(m^2+r^2k_z^2)(g/c_s^2)-rn^2/c_s^2]}{n^2[r^2(n^2/c_s^2+k_z^2)+m^2]}u_r - D\left(\frac{\rho^{(0)}r^2Du_r}{r^2(n^2/c_s^2+k_z^2)+m^2}\right) - u_rD\left(\frac{g\rho^{(0)}(r^2/c_s^2)}{r^2(n^2/c_s^2+k_z^2)+m^2}\right) - D\left(\frac{r\rho^{(0)}u_r}{r^2(n^2/c_s^2+k_z^2)+m^2}\right)+\frac{g}{n^2}u_rD\rho^{(0)}=0. \tag{6}$$

As mentioned above, Eq. (6) is valid in the entire domain so that, in this form, the variables are generalized functions. The jump condition can be obtained by integrating Eq. (6) over an infinitesimal element across the interface located at $r=r_0$:

$$-\delta\left(\frac{\rho^{(0)}r^2Du_r}{r^2(n^2/c_s^2+k_z^2)+m^2}\right)-u_{r_0}\delta\left(\frac{g\rho^{(0)}(r^2/c_s^2)}{r^2(n^2/c_s^2+k_z^2)+m^2}\right) - \delta\left(\frac{r\rho^{(0)}u_r}{r^2(n^2/c_s^2+k_z^2)+m^2}\right)+\frac{g}{n^2}u_{r_0}\delta\rho^{(0)}=0, \tag{7}$$

where $\delta f\equiv f|_{r_0+0}-f|_{r_0-0}$ is the jump of a quantity f across the interface. The radial velocity is continuous at the interface since the interface is a material surface. Thus, $u_{lr}|_{r_0}=u_{hr}|_{r_0}=u_{r_0}$. However, c_s^2, $\rho^{(0)}$, and Du_r in Eq. (7) have a jump discontinuity at the interface.

In order to emphasize the role of the parameters considered, more specifically, geometry effects and the role of the two compressibility parameters, we nondimensionalize the system as follows: $G=k_\theta/k_t$, $\tilde{k}_z=k_z/k_t=\sqrt{1-G^2}$, $\tilde{r}=rk_t$, $\tilde{r}_0=r_0k_t$, $m=G\tilde{r}_0$, $\tilde{u}_r=\sqrt{k_t/|g|}\,u_r$, $\tilde{n}^2=n^2/k_t|g|$, $\alpha_j=\rho_j/(\rho_l+\rho_h)$, and $M^2=|g|(\rho_l+\rho_h)/k_tp_0$, where $k_t=\sqrt{k_z^2+m^2/r_0^2}$.

The normalized equation for $\tilde{u}_{\tilde{r}}$ becomes, on each side of the interface,

$$D^2\tilde{u}_{\tilde{r}_j}+f_j(\tilde{r})D\tilde{u}_{\tilde{r}_j}+h_j(\tilde{r})\tilde{u}_{\tilde{r}_j}=0, \tag{8}$$

with

$$f_j(\tilde{r})=\pm\alpha_jM^2+\frac{1}{\tilde{r}}+\frac{2G^2\tilde{r}_0^2}{\tilde{r}[(\tilde{n}^2\beta_j+1-G^2)\tilde{r}^2+G^2\tilde{r}_0^2]}, \tag{9a}$$

$$h_j(\tilde{r})=\frac{[G^2\tilde{r}_0^2+\tilde{r}^2(1-G^2)]\beta_j-[(\tilde{n}^2\beta_j+1-G^2)\tilde{r}^2+G^2\tilde{r}_0^2](\alpha_jM^2+\tilde{n}^2)}{\tilde{n}^2\tilde{r}^2}+\frac{G^2\tilde{r}_0^2\pm2G^2\tilde{r}_0^2\beta_j\tilde{r}-(\tilde{n}^2\beta_j+1-G^2)\tilde{r}^2}{\tilde{r}^2[(\tilde{n}^2\beta_j+1-G^2)\tilde{r}^2+G^2\tilde{r}_0^2]} + \alpha_jM^2\beta_j\pm\frac{\alpha_jM^2}{\tilde{r}}\mp\frac{\beta_j}{\tilde{r}}. \tag{9b}$$

The stacked signs in the equations such as $\pm$ or $\mp$ distinguish between the divergent (top) and convergent (bottom) configurations and $\beta_j=\alpha_jM^2/\gamma_j$.

From Eq. (7), one obtains the normalized jump condition at the interface:

$$\left[\frac{\pm A}{\tilde{n}^2}-\frac{(\pm\beta_h\tilde{r}_0+1)\alpha_h}{(\tilde{n}^2\beta_h+1)\tilde{r}_0}+\frac{(\pm\beta_l\tilde{r}_0+1)\alpha_l}{(\tilde{n}^2\beta_l+1)\tilde{r}_0}\right]\tilde{u}_{\tilde{r}_0} - \frac{\alpha_h}{\tilde{n}^2\beta_h+1}D\tilde{u}_{h\tilde{r}}+\frac{\alpha_l}{\tilde{n}^2\beta_l+1}D\tilde{u}_{l\tilde{r}}=0. \tag{10}$$

The other boundary conditions become

$$\tilde{u}_{r_j}|_{\tilde{r}=0}=0,\quad \tilde{u}_{r_j}|_{\tilde{r}\to\infty}=0, \tag{11}$$

$$\tilde{u}_{r_l}|_{\tilde{r}=\tilde{r}_0}=\tilde{u}_{r_h}|_{\tilde{r}=\tilde{r}_0}=\tilde{u}_{r_0}. \tag{12}$$

It should be pointed out that M is the static Mach number based on the isothermal sound speed (which does not depend on γ). $M=0$ and $\gamma\to\infty$ recover UDIL and VDIL, respectively. G is a parameter characterizing the geometry, i.e., the dimension of the perturbation wavenumber space which is also the dimension of the flow space. From the definition of G, it is easily seen that $0<G<1$ represents the three-dimensional (3D) case, and $G=0$ ($m=0$) and $G=1$ ($k_z=0$) are two-dimensional (2D) cases, with the former corresponding to a 2D axisymmetric flow (r-z system) and the latter to a 2D circular flow (r-θ system). Thus, as G increases from 0 to 1, the flow changes from 2D axisymmetric to 3D cylindrical and to 2D circular.

Full analytical solutions for the growth rate have been found for several cases and are presented below.

A. Uniform density incompressible limit

In this case, $c_s^2\to\infty$ due to $p_0\to\infty$, which corresponds to $M=0$. Thus,

$$f_j(\tilde{r})=\frac{1}{\tilde{r}}+\frac{2G^2\tilde{r}_0^2}{\tilde{r}[(1-G^2)\tilde{r}^2+G^2\tilde{r}_0^2]}, \tag{13a}$$

$$h_j(\tilde{r}) = \frac{G^2\tilde{r}_0^2 - (1-G^2)\tilde{r}^2}{\tilde{r}^2[(1-G^2)\tilde{r}^2 + G^2\tilde{r}_0^2]} - \frac{(1-G^2)\tilde{r}^2 + G^2\tilde{r}_0^2}{\tilde{r}^2}. \quad (13b)$$

The corresponding normalized jump condition is

$$D\tilde{u}_{r_h}\alpha_h - D\tilde{u}_{r_l}\alpha_l + \left(\frac{1}{\tilde{r}_0} \mp \frac{1}{\tilde{n}^2}\right)A\tilde{u}_{r_0} = 0. \quad (14)$$

On each side of the interface, Eq. (8) has the solution

$$\tilde{u}_{\tilde{r}_j} = c_{j1}\frac{2^{m+1}\Gamma(2+m)[mI_m(r') + r'I_{1+m}(r')]\tilde{r}^{m-1}}{r'^m} + c_{j2}\frac{K_{m-1}(r')r' + mK_m(r')}{\tilde{r}}, \quad (15)$$

with $r' = \sqrt{(1-G^2)}\tilde{r}$ and c_{j1} and c_{j2} integral constants determined by the boundary conditions (7), (11), and (12).

After imposing the boundary conditions and eliminating the integral constants, one obtains an expression for the growth rate:

$$\tilde{n}^2 = \frac{2A}{\dfrac{(1 \mp A)K_m(r_0')}{K_{m-1}(r_0')\sqrt{1-G^2} + GK_m(r_0')} + \dfrac{(1 \pm A)I_m(r_0')}{GI_m(r_0') + \sqrt{1-G^2}I_{m+1}(r_0')}}, \quad (16)$$

with $r_0' = \sqrt{1-G^2}\tilde{r}_0$ and $K_p(r_0')$ and $I_p(r_0')$ the modified Bessel functions of the first and second kinds of order p. Note that $m = G\tilde{r}_0$ must be an integer.

For the 2D axisymmetric case ($G=0$), the growth rate reduces to

$$\tilde{n}^2 = \frac{2AK_1(\tilde{r}_0)I_1(\tilde{r}_0)}{(1 \mp A)K_0(\tilde{r}_0)I_1(\tilde{r}_0) + (1 \pm A)K_1(\tilde{r}_0)I_0(\tilde{r}_0)}, \quad (17)$$

and for 2D circular ($G=1$):

$$\tilde{n}^2 = A. \quad (18)$$

Equation (18), for the incompressible, uniform density, 2D circular case, was also obtained by Epstein.[28]

B. Varying density incompressible limit

In this case, $c_s^2 \to \infty$ due to $\gamma \to \infty$. The coefficients in the velocity perturbation equation (8) are

$$f_j(\tilde{r}) = \pm\alpha_j M^2 + \frac{1}{\tilde{r}} + \frac{2G^2\tilde{r}_0^2}{\tilde{r}[(1-G^2)\tilde{r}^2 + G^2\tilde{r}_0^2]}, \quad (19a)$$

$$h_j(\tilde{r}) = \frac{G^2\tilde{r}_0^2 - (1-G^2)\tilde{r}^2}{\tilde{r}^2[(1-G^2)\tilde{r}^2 + G^2\tilde{r}_0^2]} \pm \frac{\alpha_j M^2}{\tilde{r}} - \frac{[(1-G^2)\tilde{r}^2 + G^2\tilde{r}_0^2](\alpha_j M^2 + \tilde{n}^2)}{\tilde{n}^2\tilde{r}^2}. \quad (19b)$$

The jump condition is the same as Eq. (14). Analytical solutions are obtained for the two 2D cases, corresponding to $G=0$ and $G=1$.

$G=0$ (2D axisymmetric). The solution for the radial velocity is

$$\tilde{u}_{\tilde{r}_j} = \left[c_{j1}M_{\xi_j,1}\left(\frac{\psi_j\tilde{r}}{\tilde{r}_0}\right) + c_{j2}W_{\xi_j,1}\left(\frac{\psi_j\tilde{r}}{\tilde{r}_0}\right)\right]\frac{e^{\mp\alpha_j M^2\tilde{r}/2}}{\sqrt{\tilde{r}}}. \quad (20)$$

The corresponding dispersion relation is obtained as

$$\pm\frac{(M^2\tilde{n}^2 + 2)A\tilde{r}_0}{2\tilde{n}^2} + \frac{\alpha_h W_{\xi_h+1,1}(\psi_h)}{W_{\xi_h,1}(\psi_h)} + \frac{(3+2\xi_l)\alpha_l M_{\xi_l+1,1}(\psi_l)}{2M_{\xi_l,1}(\psi_l)} + \frac{(1+\psi_l-2\xi_l)\alpha_l + (1+\psi_h-2\xi_h)\alpha_h}{2} = 0, \quad (21)$$

with

$$\xi_j = \frac{\pm|\tilde{n}|\alpha_j M^2}{\sqrt{[(\alpha_j M^2)^2 + 4]\tilde{n}^2 + 4\alpha_j M^2}}$$

and

$$\psi_j = \frac{\sqrt{[(\alpha_j M^2)^2 + 4]\tilde{n}^2 + 4\alpha_j M^2}\tilde{r}_0}{|\tilde{n}|}.$$

$W_{j,m}(x)$ and $M_{j,m}(x)$ are the Whittaker functions.

$G=1$ (2D circular). The solution for the radial velocity is

$$\tilde{u}_{r_j} = \frac{e^{\mp\sigma_j\tilde{r}}}{\sqrt{\tilde{r}}}\left\{c_{j1}\left[I_{-1/2+A_j}\left(\frac{\sigma_j\tilde{r}}{\tilde{r}_0}\right) + I_{1/2+A_j}\left(\frac{\sigma_j\tilde{r}}{\tilde{r}_0}\right)\right] + c_{j2}\left[K_{-1/2+A_j}\left(\frac{\sigma_j\tilde{r}}{\tilde{r}_0}\right) + K_{1/2+A_j}\left(\frac{\sigma_j\tilde{r}}{\tilde{r}_0}\right)\right]\right\}. \quad (22)$$

The corresponding dispersion relation is

$$\frac{A_h-1-\sigma_h}{\sigma_h}K_{-1/2+A_h}(\sigma_h)-\frac{A_h}{\sigma_h}K_{1/2+A_h}(\sigma_h)+K_{3/2+A_h}(\sigma_h)\pm\frac{2A(G^2\tilde{r}_0\mp\tilde{n}^2)}{\alpha_h^2M^2\tilde{n}^2\tilde{r}_0}[K_{-1/2+A_h}(\sigma_h)-K_{1/2+A_h}(\sigma_h)]$$
$$-\frac{\alpha_l^2}{\alpha_2^2}\frac{K_{-1/2+A_h}(\sigma_h)-K_{1/2+A_h}(\sigma_h)}{I_{-1/2+A_l}(\sigma_l)-I_{1/2+A_l}(\sigma_l)}\left[I_{3/2+A_l}(\sigma_1)+\frac{A_l-1-\sigma_l}{\sigma_l}I_{-1/2+A_l}(\sigma_l)+\frac{A_l}{\sigma_l}I_{1/2+A_l}(\sigma_l)\right]=0, \tag{23}$$

with $A_j=\tilde{r}_0\sqrt{\alpha_jM^2+\tilde{n}^2}/\tilde{n}$ and $\sigma_j=\pm\alpha_jM^2\tilde{r}_0/2$.

C. Fully compressible flow

We have found analytical solutions to Eq. (8) for the fully compressible case only when $G=0$ (2D axisymmetric case). In this case, the radial velocity variation is obtained as

$$\tilde{u}_{\tilde{r}_j}=\left[c_{j1}M_{\eta_j,1}\left(\frac{\zeta_j\tilde{r}}{\tilde{r}_0}\right)+c_{j2}W_{\eta_j,1}\left(\frac{\zeta_j\tilde{r}}{\tilde{r}_0}\right)\right]\frac{e^{\mp\alpha_jM^2\tilde{r}/2}}{\sqrt{\tilde{r}}}. \tag{24}$$

The corresponding dispersion relation is

$$\pm A\tilde{r}_0\left[\frac{\tilde{n}^2\beta_h+1}{\tilde{n}^2}+\frac{M^2}{2(\tilde{n}^2\beta_l+1)}\right]+\frac{\alpha_hW_{\eta_h+1,1}(\zeta_h)}{W_{\eta_h,1}(\zeta_h)}-\frac{(\zeta_h-2\eta_h\pm2\beta_h\tilde{r}_0+1)\alpha_h}{2}$$
$$\pm\frac{M^2\tilde{r}_0\tilde{n}^2(\alpha_h^2\beta_l-\alpha_1^2\beta_h)}{2(\tilde{n}^2\beta_l+1)}\frac{(\zeta_h-2\eta_h\pm2\beta_h\tilde{r}_0+1)\alpha_h}{2}\frac{\tilde{n}^2\beta_h+1}{\tilde{n}^2\beta_l+1}+\left(\frac{3}{2}+\eta_l\right)\frac{\alpha_lM_{\eta_l+1,1}(\zeta_l)}{M_{\eta_l,1}(\zeta_l)}\frac{\tilde{n}^2\beta_h+1}{\tilde{n}^2\beta_l+1}=0, \tag{25}$$

with

$$\eta_j=\frac{\pm|\tilde{n}|(\alpha_jM^2-\beta_j)}{\sqrt{4\tilde{n}^4\beta_j+[(\alpha_jM^2)^2+4]\tilde{n}^2+4(\alpha_jM^2-\beta_j)}}$$

and

$$\zeta_j=\frac{\sqrt{4\tilde{n}^4\beta_j+[(\alpha_jM^2)^2+4]\tilde{n}^2+4(\alpha_jM^2-\beta_j)}\tilde{r}_0}{|\tilde{n}|}.$$

IV. RESULTS AND DISCUSSIONS

In this section, the growth rate dependences on various parameters are examined. The results are grouped into three categories: (1) compressibility effects as characterized by the static Mach number M and the ratio of specific heats, γ, (2) geometry effects due to the nature of the cylindrical geometry, and (3) differences between the convergent and divergent configurations. To obtain the growth rate, Eq. (8), together with the boundary and jump conditions, was integrated using a fourth-order Runge–Kutta scheme. The cases where analytical solutions were found are used to verify the numerical scheme.

A. Compressibility effects

$\tilde{n}_{cc}^2$, $\tilde{n}_{cu}^2$, and $\tilde{n}_{cv}^2$ are used to denote the normalized rates of growth (by $k_t|g|$) corresponding to the fully compressible flow, UDIL, and VDIL. As explained above, compressibility effects are characterized by the fluid property γ and flow property M, with large M corresponding to more compressible flow and small γ to more compressible fluid.

In general, if $\tilde{r}_0$ is not very small, the compressible growth rate is bounded by the growth rates obtained for UDIL and VDIL, similar to the PI case in the Cartesian geometry[8] (Fig. 1). Thus, the growth rate decreases for more compressible flows (characterized by smaller $1/M$) and increases for more compressible fluids (characterized by lower γ). In all cases, the UDIL growth rate is recovered as $1/M\to\infty$.

The growth rate variation due to compressibility can be

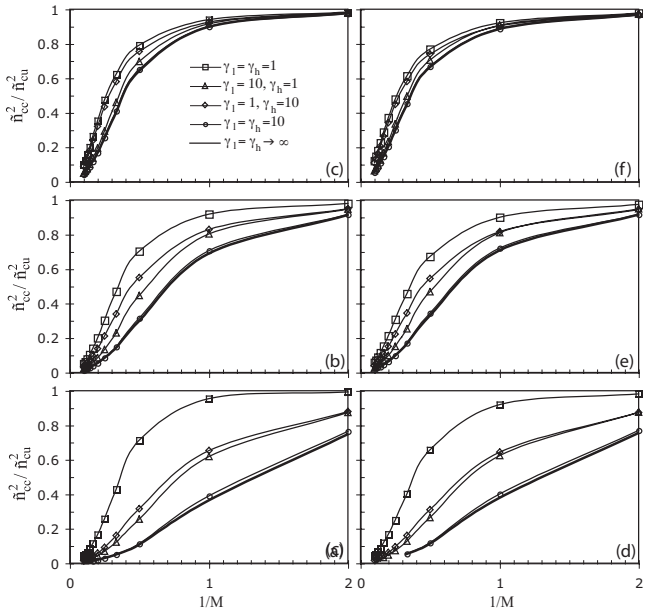

FIG. 1. Compressible to UDIL growth rate ratio as a function of $1/M$ for the convergent (left column) and divergent (right column) configurations for different γ_l and γ_h combinations at $G=0.5$, $\tilde{r}_0=2.0$. The pure solid line corresponds to $\tilde{n}_{cv}^2/\tilde{n}_{cu}^2$. [(a) and (d)] $A=0.2$, [(b) and (e)] $A=0.5$, and [(c) and (f)] $A=0.8$.

explained intuitively by calculating the changes in the local A due to nonuniform equilibrium densities on the two sides of the interface. As the flow compressibility increases, the change in the equilibrium density variation leads to a decrease in the local A for points on the interface situated above the initial position and an increase in the local A for points on the interface situated below the initial position. However, the change in the local A is larger above the initial position of the interface so that the overall effect is a decrease in the average A. This suggests a stabilizing effect of compressibility when this is characterized by changes in the flow conditions (represented here by M). On the other hand, as γ decreases, the equilibrium density and pressure remain unchanged. As the heavy fluid falls towards regions with higher pressures, its volume decreases progressively more at higher γ, so that the tips of the spikes fall less for more compressible fluids. Similarly, the tips of the bubbles rise more for fluids with higher γ. The change is larger for the bubbles, so that the overall effect is an increase in the rate of growth due to compressibility when this is characterized by changes in the fluid properties (represented here by γ). The arguments imply not only opposite influence of the two compressibility parameters on the growth rate but also on the spike and bubble sides, leading to an asymmetry of the layer in the compressible case larger than the overall effect on the growth rate. This effect is being verified with direct numerical simulations of the fully nonlinear case and will be reported elsewhere.

Figure 1 also shows that the compressible growth rate is more sensitive to changes in γ for the light fluid (compare the results obtained for $\gamma_l=10$, $\gamma_h=1$ and $\gamma_l=1$, $\gamma_h=10$ with the perfectly compressible case $\gamma_l=1$, $\gamma_h=1$) which is consistent with the arguments above that the changes to the tips of the bubbles position influence more the overall growth rate. The results are also sensitive to the A values. At large A, the growth rate shows little sensitivity to changes in the ratios of specific heats and takes values close to the VDIL growth rate.

Overshooting (n_{cc}^2 exceeds n_{cu}^2) occurs in both convergent and divergent configurations when $\tilde{r}_0$ is small (Fig. 2). In this case, the arguments above with regard to changes in the local A due to compressibility are no longer valid. They were based on small amplitude expansions in the equilibrium density profile which can no longer be made in the interior domain. Small values of $\tilde{r}_0$ can be obtained only in the 2D axisymmetric ($G=0$) and some 3D (with small G) cases. Overshooting is also observed in the Cartesian geometry when the domain size of the heavy fluid is much smaller than the wavelength of the perturbation and $\gamma_l \approx 1$.[8] Here, the condition $\gamma \approx 1$ is required only for the convergent configuration; for the divergent arrangement it can occur at all values of γ. The effect is more distinctive than obtained in the Cartesian geometry and becomes more pronounced at low A for the convergent and of high A for the divergent cases. Undershooting (n_{cc}^2 drops below n_{cv}^2) may occur at large γ, small A, and small $1/M$ (highly compressible flow) but is much less pronounced than overshooting and not discussed here.

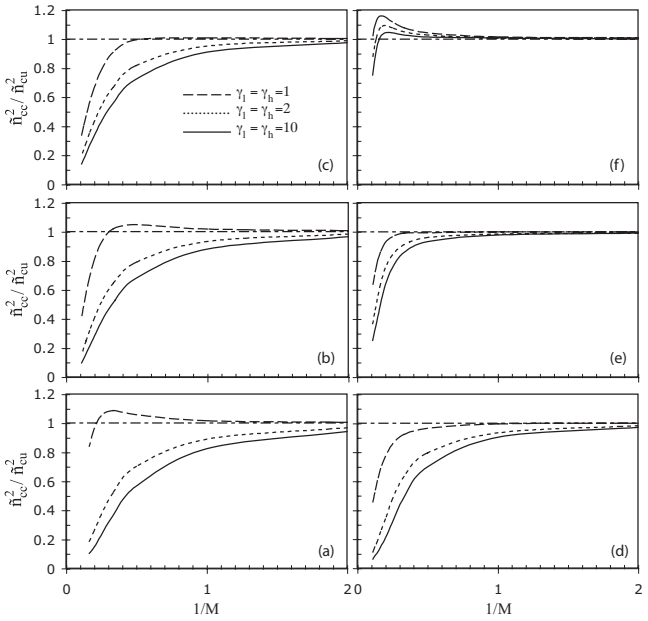

FIG. 2. Compressible to UDIL growth rate ratio for the convergent (left column) and divergent (right column) cases as a function of $1/M$ for different γ values at $G=0$, $\tilde{r}_0=0.1$. [(a) and (d)] $A=0.2$, [(b) and (e)] $A=0.5$, and [(c) and (f)] $A=0.8$.

B. Geometry effects

To characterize the geometry effects, the influences of different parameters on the ratio n_{cc}^2/n_{pc}^2 of the growth rates obtained for CI and PI are now discussed. For meaningful comparisons, the PI configuration corresponds to a finite domain with size $\tilde{r}_0$ occupied by the heavy fluid in the divergent configuration and by the light fluid in the convergent case and an infinite domain occupied by the other fluid. Corresponding dispersion relations obtained for the PI as special half-infinite cases are given in the Appendix.

For UDIL, the growth rate ratio being discussed has an analytical formula:

$$\frac{\tilde{n}_{cc}^2}{\tilde{n}_{pc}^2} = \frac{2B_I B_K}{(1 \mp A)K_m(r_0')B_I + (1 \pm A)I_m(r_0')B_K} \frac{e^{\tilde{r}_0} \pm Ae^{-\tilde{r}_0}}{e^{\tilde{r}_0} - e^{-\tilde{r}_0}}, \tag{26}$$

with $B_I = GI_m(r_0') + \sqrt{1-G^2}I_{m+1}(r_0')$ and $B_K = GK_m(r_0') + \sqrt{1-G^2}K_{m-1}(r_0')$.

For 2D axisymmetric ($G=0$) Eq. (26) reduces to

$$\frac{\tilde{n}_{cc}^2}{\tilde{n}_{pc}^2} = \frac{2K_1(\tilde{r}_0)I_1(\tilde{r}_0)}{(1 \mp A)K_0(\tilde{r}_0)I_1(\tilde{r}_0) + (1 \pm A)K_1(\tilde{r}_0)I_0(\tilde{r}_0)} \times \frac{e^{\tilde{r}_0} \pm Ae^{-\tilde{r}_0}}{e^{\tilde{r}_0} - e^{-\tilde{r}_0}} \tag{27}$$

and for 2D circular ($G=1$) to

$$\frac{\tilde{n}_{cc}^2}{\tilde{n}_{pc}^2} = \frac{e^{\tilde{r}_0} \pm Ae^{-\tilde{r}_0}}{e^{\tilde{r}_0} - e^{-\tilde{r}_0}}. \tag{28}$$

Figure 3 shows the importance of the compressibility effects on the ratio n_{cc}^2/n_{pc}^2 for a representative 3D case ($G=0.5$) and $\tilde{r}_0=2$. The CI growth rate is larger for the conver-

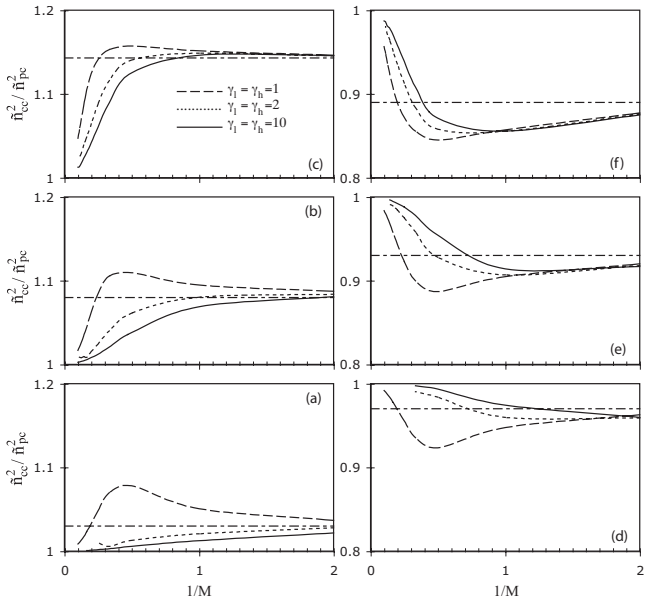

FIG. 3. Ratio of the CI vs PI growth rates for the convergent (left column) and divergent (right column) configurations as a function of $1/M$ for different γ values at $\tilde{r}_0=2.0$, $G=0.5$. The dash-dotted lines are the corresponding asymptotic UDIL values. [(a) and (d)] $A=0.2$, [(b) and (e)] $A=0.5$, and [(c) and (f)] $A=0.8$.

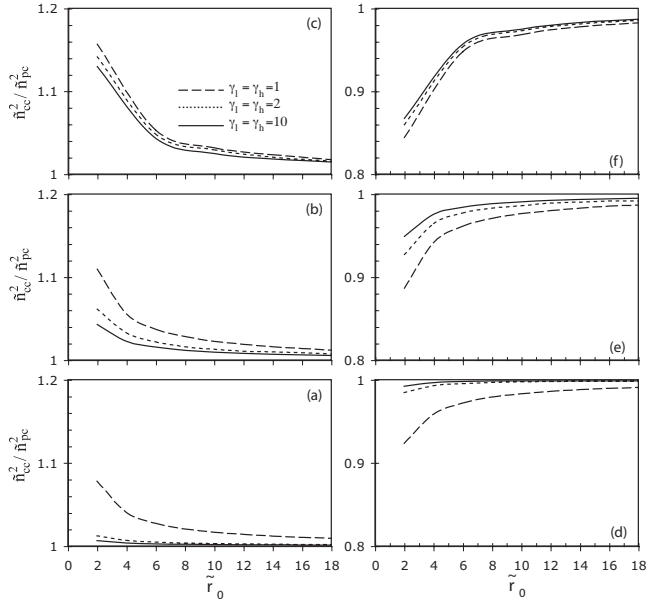

FIG. 4. Ratio of the CI vs PI growth rates for the convergent (left column) and divergent (right column) configurations; dependence on $\tilde{r}_0$ for different γ values at $G=0.5$, $M=2$. [(a) and (d)] $A=0.2$, [(b) and (e)] $A=0.5$, and [(c) and (f)] $A=0.8$.

gent configuration than the PI growth rate but slower for the divergent case. At moderate values of γ, it seems that there is a critical value of M ($M \approx 2$ for $\gamma=1$) at which the difference between the CI and PI growth rates is largest. This difference also increases with A. The ratio of the CI versus PI growth rates depends sensibly on the values of γ only for highly compressible flows. For $M<1$, γ influence is less important. Similar behavior is observed in the 2D axisymmetric case. However, in the 2D circular case, the behavior is more complicated: n_{cc}^2 can be either larger or smaller than n_{pc}^2 depending on the combinations among parameters (see also below).

As the normalized radius $\tilde{r}_0 \to \infty$, the growth rate should recover the PI growth rate. For finite values of $\tilde{r}_0$, the CI growth rate is always larger for the convergent and smaller for the divergent configuration than the corresponding PI growth rate (Fig. 4). Again, the difference between the CI and PI growth rates increases with A. At large A, however, this difference depends less sensibly on the ratios of specific heats. The results remain qualitatively the same for the axisymmetric case but may change for the 2D circular case.

The dimensionality parameter G increases from 0 to 1 as the flow changes from 2D axisymmetric ($G=0$) to 3D cylindrical ($0<G<1$) and to 2D circular ($G=1$). Figure 5 shows that the CI to PI growth rate ratio behaves qualitatively the same at small and moderate values of G as a function of γ but becomes different when G is close to 1. At low A, the divergent/convergent results described above also change qualitatively at large values of G. Thus, 2D circular or 3D with small k_z calculations do not represent a useful model for the fully 3D cylindrical case. Nevertheless, the results obtained for the 2D axisymmetric case are qualitatively the same as those obtained for the 3D cylindrical domain.

C. Convergence versus divergence effects

As pointed out above, the growth rates obtained for the convergent and divergent configurations change qualitatively when compared to the PI case. Below, the growth rates obtained for the two unstable configurations are compared directly to the CI case. The fluid arrangements for the two cases are explained again for clarity—convergence corresponds to infinite heavy fluid domain pressing a finite light fluid domain due to inward acceleration, while divergence corresponds to a finite heavy fluid domain expelling an infi-

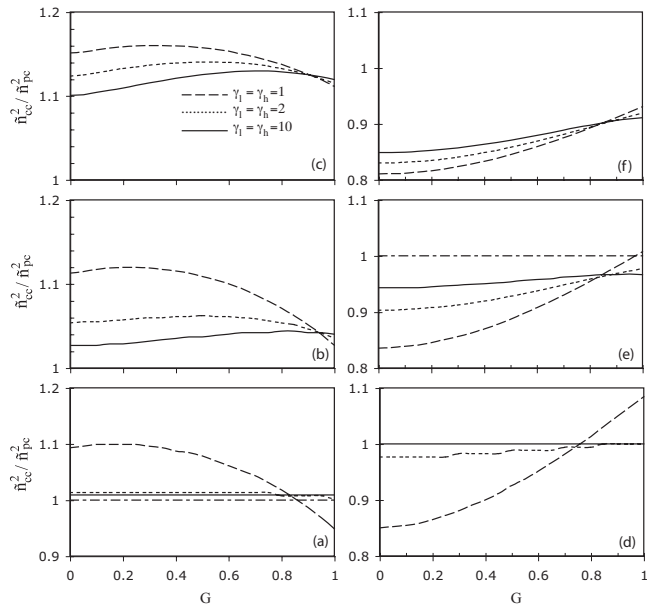

FIG. 5. Ratio of the CI vs PI growth rates for the convergent (left column) and divergent (right column) configurations as a function of G for different γ values at $M=2$, $\tilde{r}_0=2$. [(a) and (d)] $A=0.2$, [(b) and (e)] $A=0.5$, and [(c) and (f)] $A=0.8$.

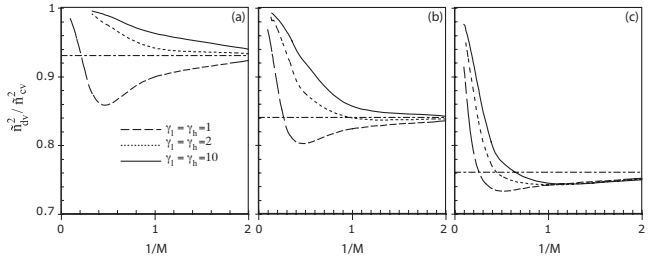

FIG. 6. Ratio of the divergent vs convergent configuration growth rate dependence on $1/M$ at $\tilde{r}_0=2$, $G=0.5$ for different γ values. The dash-dotted lines are the corresponding asymptotic UDIL values. (a) $A=0.2$, (b) $A=0.5$, and (c) $A=0.8$.

nite light fluid domain due to an outward acceleration. The ratio $\tilde{n}^2_{dv}/\tilde{n}^2_{cv}$ is used to quantitatively express the difference between the divergent and convergent configuration growth rates for a CI setup.

For UDIL, $\tilde{n}^2_{dv}/\tilde{n}^2_{cv}$ is given analytically by

$$\frac{\tilde{n}^2_{dv}}{\tilde{n}^2_{cv}}=\frac{\alpha_h K_m(r_0')B_I+\alpha_l I_m(r_0')B_K}{\alpha_l K_m(r_0')B_I+\alpha_h I_m(r_0')B_K}, \tag{29}$$

which for the 2D axisymmetric case ($G=0$), reduces to

$$\frac{\tilde{n}^2_{dv}}{\tilde{n}^2_{cv}}=\frac{\alpha_h K_0(\tilde{r}_0)I_1(\tilde{r}_0)+\alpha_l I_0(\tilde{r}_0)K_1(\tilde{r}_0)}{\alpha_l K_0(\tilde{r}_0)I_1(\tilde{r}_0)+\alpha_h I_0(\tilde{r}_0)K_1(\tilde{r}_0)} \tag{30}$$

and for the 2D circular case ($G=1$) to

$$\tilde{n}^2_{dv}/\tilde{n}^2_{cv}=1. \tag{31}$$

For all 3D cylindrical cases, the growth rate obtained for the divergent arrangement is smaller than that obtained for the convergent arrangement and the difference increases with A (Fig. 6). Again, at small values of γ, there seems to be a critical M at which the difference between the divergent and convergent configuration growth rates is largest. This critical M changes little with A and takes values close to 2. As before, the γ influence is sensibly felt for highly compressible flows ($M>1$).

For large values of $\tilde{r}_0$ the curvature effects become small (Fig. 7) and the ratio $\tilde{n}^2_{dv}/\tilde{n}^2_{cv}$ is close to the PI interface result. For PI, the divergent and convergent arrangement growth rates, while having the same qualitative behavior, are close to 1. Thus, the differences between the two growth rates are the largest for small $\tilde{r}_0$. γ influence on $\tilde{n}^2_{dv}/\tilde{n}^2_{cv}$ is also largest at small $\tilde{r}_0$; however, it is significant only at small A. Again, the results change qualitatively at large G ($G>0.8$) when the flow becomes close to the 2D circular case: it is seen that $\tilde{n}^2_{dv}$ can exceed $\tilde{n}^2_{cv}$ and the influences of γ and A become the opposite of those obtained at low to moderate G. This further emphasizes that the 2D circular limit does not represent a useful model for the fully 3D cylindrical case.

V. SUMMARY AND CONCLUSION

A linear stability analysis of the RTI in cylindrical geometry with CI is performed to study (1) the effects of compressibility, (2) the geometry as related to the difference between PI and CI configurations and also to the difference

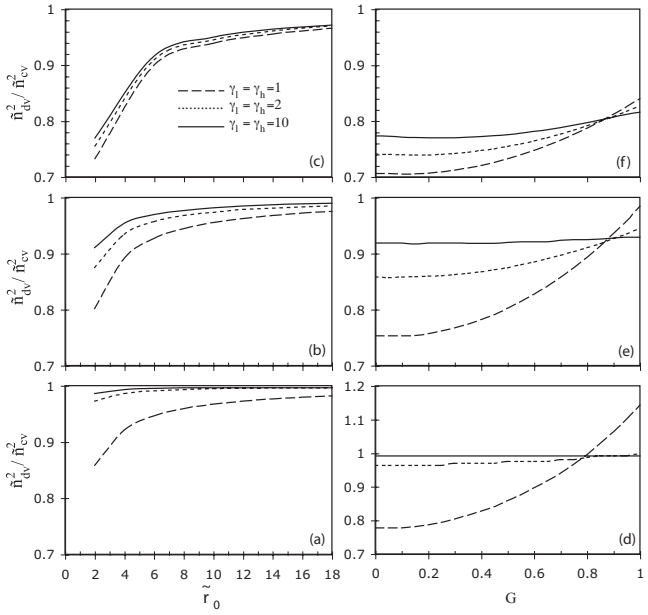

FIG. 7. Dependence of $\tilde{n}^2_{dv}/\tilde{n}^2_{cv}$ on $\tilde{r}_0$ (left column, $G=0.5$, $M=2$) and G (right column, $M=2$, $\tilde{r}_0=2$) for different γ values. [(a) and (d)] $A=0.2$, [(b) and (e)] $A=0.5$, and [(c) and (f)] $A=0.8$.

between the 2D and 3D cases, and (3) the distinction between the convergent (gravity acting inward) and divergent (gravity acting outward) unstable arrangements. The flow is considered inviscid and compressible. Full analytical solutions are found in several limiting cases. For the fully compressible case analytical results are obtained for the 2D axisymmetric configuration. For the rest of the cases, the linearized equations are solved numerically to obtain the growth rates.

The main findings are as follows:

- Compressibility can be characterized by two parameters, a static Mach number M (a flow feature) and the ratio of specific heats, γ (a fluid feature). The limiting incompressible flows (defined by zero divergence of velocity) can be obtained as either $M\to 0$ or as $\gamma\to\infty$ and can be different in the two cases. Thus, as $M\to 0$ the density becomes uniform while as $\gamma\to\infty$ density variations are allowed. For equilibrium initial conditions (both hydrodynamic and thermal) the compressible growth rate was found to be bounded, in general, by the growth rates obtained for the UDIL from above and for the VDIL from below. Similar to the PI case,[8] the growth rate decreases as M increases (more compressible flow) but increases as γ decreases (more compressible fluid). Overshooting (compressible growth rate larger than UDIL growth rate) can occur when the normalized radius of the interface is very small, which is possible only in the 2D axisymmetric and 3D cylindrical with small tangential wavenumber configurations. This effect is more pronounced than for the PI case. Undershooting (compressible growth rate smaller than VDIL growth rate) can also occur but is less significant.
- Compressibility effects, as characterized by γ, are

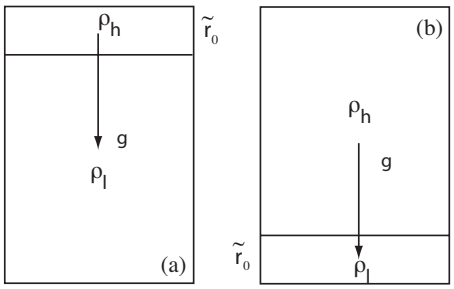

FIG. 8. Schematic PI cases corresponding to (a) divergent and (b) convergent CI cases.

mostly felt at low A. In this case, the growth rate is more sensible to changes in γ values of the lighter fluid. At high A, the γ influence becomes small.

- For the 3D case, instability grows faster for the convergent than for the divergent arrangement. The differences between the two unstable configuration growth rates are small for PI but become significant for CI. They are also amplified at high A and small values of γ.
- For low values of γ there seems to be a critical value of M at which the difference between the divergent and convergent configuration growth rates as well as the growth rates obtained for the CI and PI cases is the largest.
- The wavenumbers of the perturbations in tangential and axial directions have different influences on the growth rate. The differences can be captured by a dimensionality parameter G, which varies between 0 when $k_\theta=0$ to 1 when $k_z=0$. Thus, as G increases from 0 to 1, the flow changes from 2D axisymmetric ($G=0$) to 3D cylindrical ($0<G<1$) and to 2D circular ($G=1$). All the 3D cylindrical results remain qualitatively the same in the 2D axisymmetric case but change qualitatively as the flow becomes close to the 2D circular configuration ($k_\theta \gg k_z$). In this case, the influences of A and γ are opposite than for the 3D cylindrical case and the growth rate for the divergent configuration exceeds that obtained for the convergent arrangement. Thus, 2D circular case calculations do not represent a useful model for the fully 3D cylindrical case, while the influences of the parameters considered remain qualitatively the same as the flow changes from 3D cylindrical to 2D axisymmetric.

The findings above are currently being examined in the fully nonlinear case and the results will be published elsewhere.

APPENDIX: DISPERSION RELATIONS FOR PLANAR INTERFACE

Analytical dispersion relations for the RTI growth rate in the Cartesian geometry with PI are obtained from Eq. (26) in Ref. 8 and given here for completeness. Two special cases, schematically shown in Fig. 8, are considered by analogy to the two cylindrical unstable arrangements: the convergent configuration, corresponding to infinite heavy fluid domain versus finite light fluid domain, and the divergent configuration, corresponding to infinite light fluid domain versus finite heavy fluid domain. The normalized dispersion relations are as follows.

Fully compressible flow. We define $A_{\mp}=0.5(1\mp A)M^2$, $a_u=[(1+A)\gamma_h(\gamma_l+A_-\tilde{n}_p^2)-(1-A)\gamma_l(\gamma_h+A_+\tilde{n}_p^2)]$, $b_{dl}=(1-A)\gamma_l(\gamma_h+A_+\tilde{n}^2)$, $b_{dh}=(1+A)\gamma_h(\gamma_l+A_-\tilde{n}^2)$, and

$$\lambda_l^{\pm}=\frac{A_-}{2}\pm\sqrt{1+\frac{\tilde{n}_p^2A_-}{\gamma_1}+\frac{\gamma_1-1}{\gamma_1}\frac{A_-}{\tilde{n}_p^2}+\frac{A_-^2}{4}}, \tag{A1a}$$

$$\lambda_h^{\pm}=\frac{A_+}{2}\pm\sqrt{1+\frac{\tilde{n}_p^2A_+}{\gamma_h}+\frac{\gamma_h-1}{\gamma_h}\frac{A_+}{\tilde{n}_p^2}+\frac{A_+^2}{4}}, \tag{A1b}$$

- Infinite light fluid domain [Fig. 8(a)] corresponding to the divergent CI case:

$$\tilde{n}_{pc}^2=\frac{(e^{-\lambda_h^+\tilde{r}_0}-e^{-\lambda_h^-\tilde{r}_0})a_u}{b_{dl}\lambda_l^+(e^{-\lambda_h^+\tilde{r}_0}-e^{-\lambda_h^-\tilde{r}_0})-b_{dh}(\lambda_h^+e^{-\lambda_h^+\tilde{r}_0}-\lambda_h^-e^{-\lambda_h^-\tilde{r}_0})}. \tag{A2}$$

- Infinite heavy fluid domain [Fig. 8(b)] corresponding to the convergent CI case:

$$\tilde{n}_{pc}^2=\frac{(e^{-\lambda_l^+\tilde{r}_0}-e^{-\lambda_l^-\tilde{r}_0})a_u}{b_{dl}(\lambda_l^+e^{\lambda_l^+\tilde{r}_0}-\lambda_l^-e^{\lambda_l^-\tilde{r}_0})-b_{dh}\lambda_h^-(e^{-\lambda_l^+\tilde{r}_0}-e^{-\lambda_l^-\tilde{r}_0})}. \tag{A3}$$

VDIL. In the VDIL, Eqs. (A1a), (A1b), (A3), (A4a), and (A4b) reduce to

$$\lambda_l^{\pm}=\frac{A_-}{2}\pm\sqrt{1+\frac{A_-}{\tilde{n}_p^2}+\frac{A_-^2}{4}}, \tag{A4a}$$

$$\lambda_h^{\pm}=\frac{A_+}{2}\pm\sqrt{1+\frac{A_+}{\tilde{n}_p^2}+\frac{A_+^2}{4}}, \tag{A4b}$$

- Infinite light fluid domain [Fig. 8(a)] corresponding to the divergent CI case:

$$\tilde{n}_{pc}^2=\frac{A(e^{-\lambda_h^+\tilde{r}_0}-e^{-\lambda_h^-\tilde{r}_0})}{\alpha_l\lambda_l^+(e^{-\lambda_h^+\tilde{r}_0}-e^{-\lambda_h^-\tilde{r}_0})-\alpha_h(\lambda_h^+e^{-\lambda_h^+\tilde{r}_0}-\lambda_h^-e^{-\lambda_h^-\tilde{r}_0})}. \tag{A5}$$

- Infinite heavy fluid domain [Fig. 8(b)] corresponding to the convergent CI case:

$$\tilde{n}_{pc}^2=\frac{A(e^{-\lambda_l^+\tilde{r}_0}-e^{-\lambda_l^-\tilde{r}_0})}{\alpha_l(\lambda_l^+e^{\lambda_l^+\tilde{r}_0}-\lambda_l^-e^{\lambda_l^-\tilde{r}_0})-\alpha_h\lambda_h^-(e^{-\lambda_l^+\tilde{r}_0}-e^{-\lambda_l^-\tilde{r}_0})}. \tag{A6}$$

UDIL. In this case, the dispersion relations simply reduce to the following.

- Infinite light fluid domain:

$$\tilde{n}_{pu}^2=\frac{A(e^{\tilde{r}_0}-e^{-\tilde{r}_0})}{e^{\tilde{r}_0}+Ae^{-\tilde{r}_0}}. \tag{A7}$$

- Infinite heavy fluid domain:

$$\tilde{n}_{pu}^2 = \frac{A(e^{\tilde{r}_0} - e^{-\tilde{r}_0})}{e^{\tilde{r}_0} - Ae^{-\tilde{r}_0}}. \tag{A8}$$

[1] G. I. Taylor, "Instability of liquid surfaces when accelerated in a direction perpendicular to their planes," Proc. R. Soc. London, Ser. A **201**, 192 (1950).
[2] D. H. Sharp, "An overview of Rayleigh–Taylor instability," Physica D **12**, 3 (1984).
[3] S. Chandrasekhar, *Hydrodynamic and Hydromagnetic Stability*, International Series of Monographs on Physics (Dover, New York, 1981).
[4] P. O. Vandervoort, "The character of the equilibrium of a compressible, inviscid fluid of varying density," Astrophys. J. **134**, 699 (1961).
[5] I. B. Bernstein and D. L. Book, "Effect of compressibility on the Rayleigh–Taylor instability," Phys. Fluids **26**, 453 (1983).
[6] Y. Yang and Q. Zhang, "General properties of a multilayer stratified fluids system," Phys. Fluids A **5**, 1167 (1993).
[7] L. Turner, "Rayleigh–Taylor instabilities and gravity waves in compressible fluids," Los Alamos National Laboratory Report No. LA-UR-02-6439, 2002.
[8] D. Livescu, "Compressibility effects on the Rayleigh–Taylor instability growth between immiscible fluids," Phys. Fluids **16**, 118 (2004).
[9] N. Masmoudi, "Asymptotic problems and compressible-incompressible limit," in *Advances in Mathematical Fluid Mechanics*, edited by J. Malek, J. Necas, and M. Rokyta (Springer, New York, 2000), pp. 119–158.
[10] J. Leray, "Etude de diverses equations integrales nonlineaires et de quelques problemes que pose l'hydrodynamique," J. Math. Pures Appl. **12**, 1 (1933).
[11] A. Burrows, "Supernova explosions in the Universe," Nature (London) **403**, 727 (2000).
[12] J. D. Lindl, *Inertial Confinement Fusion* (Springer, New York, 1998).
[13] J. D. Lindl, P. Amendt, R. L. Berger, S. G. Glendinning, S. H. Glenzer, S. W. Haan, R. L. Kauffman, and O. L. Landen, "The physics basis for ignition using indirect-drive targets on the National Ignition Facility," Phys. Plasmas **11**, 339 (2004).
[14] K. Robinson, L. J. Dursi, P. M. Ricker, R. Rosner, A. C. Calder, M. Zingale, J. W. Truran, T. Linde, A. Caceres, B. Fryxell, K. Olson, K. Riley, A. Siegel, and N. Vladimirova, "Morphology of rising hydrodynamic and magnetohydrodynamic bubbles from numerical simulations," Astrophys. J. **601**, 621 (2004).
[15] G. I. Bell, "Taylor instability on cylinders and spheres in the small amplitude approximation," Los Alamos Scientific Laboratory Report No. LA-1321, 1951.
[16] M. S. Plesset, "On the stability of fluid flows with spherical symmetry," J. Appl. Phys. **25**, 96 (1954).
[17] J. B. Beck, "The effects of convergent geometry on the ablative Rayleigh–Taylor instability in cylindrical implosions," Ph.D. thesis, Purdue University, 1996.
[18] W. W. Hsing and N. M. Hoffman, "Measurement of feedthrough and instability growth in radiation-driven cylindrical implosion," Phys. Rev. Lett. **78**, 3876 (1997).
[19] X. M. Chen, V. E. Schrock, and P. F. Peterson, "Rayleigh–Taylor instability of cylindrical jets with radial motion," Nucl. Eng. Des. **177**, 121 (1997).
[20] K. O. Mikaelian, "Stability and mix in spherical geometry," Phys. Rev. Lett. **65**, 992 (1990).
[21] K. O. Mikaelian, "Rayleigh–Taylor and Richtmyer–Meskov instabilities and mixing in stratified spherical shells," Phys. Rev. A **42**, 3400 (1990).
[22] K. O. Mikaelian, "Rayleigh–Taylor and Richtmyer–Meskov instabilities and mixing in stratified cylindrical shells," Phys. Fluids **17**, 094105 (2005).
[23] P. Amendt, "Bell–Plesset effects for an accelerating interface with contiguous density gradients," Phys. Plasmas **13**, 042702 (2006).
[24] S. J. Han, "Stability of an expanding cylindrical plasma envelope: Rayleigh–Taylor instability," Phys. Fluids **25**, 1724 (1982).
[25] S. J. Han and B. R. Sundam, "Hydrodynamic instability in an imploding cylindrical plasma shell," Phys. Rev. A **26**, 926 (1982).
[26] J. N. Shiau, E. B. Goldman, and C. I. Weng, "Linear stability analysis of laser-driven spherical implosions," Phys. Rev. Lett. **32**, 352 (1974).
[27] F. Hattori, H. Takabe, and K. Mima, "Rayleigh–Taylor instability in a spherically stagnating system," Phys. Fluids **29**, 1719 (1986).
[28] R. Epstein, "On the Bell–Plesset effects: The effects of the uniform compression and geometrical convergence on the classical Rayleigh–Taylor instability," Phys. Plasmas **11**, 5114 (2004).
[29] H. Takabe, L. Montierth, and R. L. Morse, "Self-consistent eigenvalue analysis of Rayleigh–Taylor instability in an ablating plasma," Phys. Fluids **26**, 2299 (1983).
[30] D. Livescu, "Comment on 'Compressible Rayleigh–Taylor instability in supernova remnants' ," Phys. Fluids **17**, 069101 (2005); "Reply to 'Response to "Comment on 'Compressible Rayleigh–Taylor instability in supernova remnants' " ' ," *ibid.* **17**, 089101 (2005).
[31] R. C. Reid, J. M. Prausnitz, and T. K. Sherwood, *The Properties of Gases and Liquids* (McGraw-Hill, New York, 1977).